Accepted Manuscript

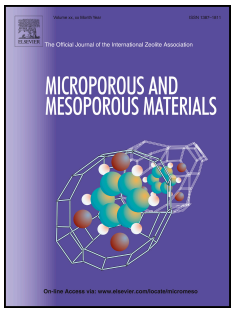

Oxidative dehydrogenation of ethylbenzene over CMK-1 and CMK-3 carbon replicas with various mesopore architectures

Sebastian Jarczewski, Marek Drozdek, Piotr Michorczyk, Carlos Cuadrado-Collados, Jesus Gandara-Loe, Joaquín Silvestre-Albero, Piotr Kuśtrowski

PII: S1387-1811(18)30315-9

DOI: 10.1016/j.micromeso.2018.06.007

Reference: MICMAT 8960

To appear in: *Microporous and Mesoporous Materials*

Received Date: 3 April 2018

Revised Date: 4 May 2018

Accepted Date: 3 June 2018

Please cite this article as: S. Jarczewski, M. Drozdek, P. Michorczyk, C. Cuadrado-Collados, J. Gandara-Loe, Joaquí. Silvestre-Albero, P. Kuśtrowski, Oxidative dehydrogenation of ethylbenzene over CMK-1 and CMK-3 carbon replicas with various mesopore architectures, *Microporous and Mesoporous Materials* (2018), doi: 10.1016/j.micromeso.2018.06.007.

Structure shrinkage

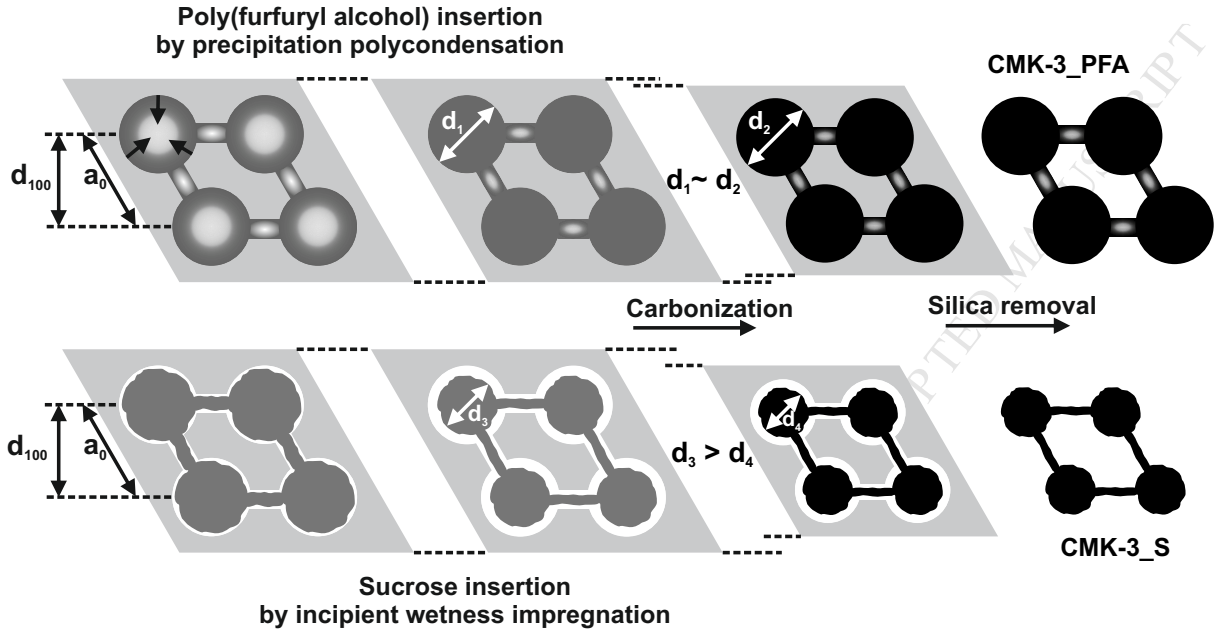

Oxidative dehydrogenation of ethylbenzene

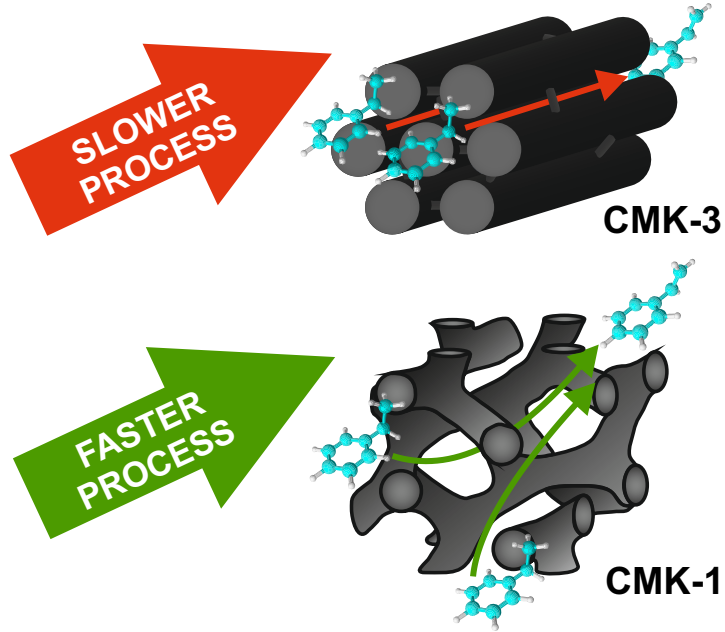

Oxidative dehydrogenation of ethylbenzene over CMK-1 and CMK-3 carbon replicas with various mesopore architectures

Sebastian Jarczewski[a], Marek Drozdek[a], Piotr Michorczyk[b], Carlos Cuadrado-Collados[c], Jesus Gandara-Loe[c], Joaquín Silvestre-Albero[c], Piotr Kuśtrowski[a,*]

[a]*Department of Chemical Technology, Faculty of Chemistry, Jagiellonian University, Gronostajowa 2, 30-387 Kraków, Poland*

[b]*Institute of Organic Chemistry and Technology, Cracow University of Technology, Warszawska 24, 31-155 Kraków, Poland*

[c]*Laboratorio de Materiales Avanzados, Departamento de Química Inorgánica-Instituto Universitario de Materiales, Universidad de Alicante, Ctra. San Vicente-Alicante s/n, E-03690 San Vicente del Raspeig, Spain*

Abstract

Nanoreplication strategy was used for the synthesis of mesoporous ordered carbon materials with various pore architectures and surface compositions. Two different silica templates (regular MCM-48 and hexagonal SBA-15) were filled with a carbon precursor – poly(furfuryl alcohol) or sucrose – by the precipitation polycondensation or incipient wetness impregnation, respectively. Furthermore, the resulting carbon precursors/silica composites were carbonized at various temperatures from the range of 650-1050 °C. It was shown that the carbon precursor and method of its deposition strongly influenced structural and textural parameters of the final carbon material determined by XRD, low-temperature N_2 adsorption and TEM. The specific surface

* Corresponding author. Tel: +48 12 6862415. E-mail: piotr.kustrowski@uj.edu.pl (Piotr Kuśtrowski)

area of the sucrose-based CMK-3 was ca. 45 % higher than the poly(furfuryl alcohol)-derived replicas. On the other hand, this effect was not observed for CMK-1 replicas. The carbonization temperatures tuned up the content of C=O moieties on the surface of carbon replica calculated based on temperature-programmed desorption (TPD) profiles. Obviously, the concentration of C=O functionalities was correlated to the catalytic activity in the oxidative dehydrogenation of ethylbenzene (EB) to styrene. Nevertheless, the CMK-1 replicas were more sensitive to the C=O concentration in terms of EB conversion. Hence, we discussed carefully the role of the pore geometry in the catalytic performance of the studied carbon materials. For the CMK-1 and CMK-3 carbon replicas with comparable chemical and textural properties, but different pore structure, the initial EB conversion varied considerably, reaching 34.2 % and 21.6 %, respectively, at 350 °C and EB/O_2 ratio = 1.0.

Keywords: ordered mesoporous carbon, CMK-1, CMK-3, oxidative dehydrogenation, ethylbenzene

1. Introduction

A family of metal-free carbon catalysts has attracted widespread interest, because of remarkable catalytic properties and environmentally friendly character, which is in agreement with the concept of green chemistry and sustainable development [1-3]. However, an implementation of these materials to the industrial practice depends on a development of adequately active, selective and stable catalysts. Nanostructured carbons combining unique properties (i.e. high specific surface area providing a large number of superficial active sites) and relatively low cost of production have drawn

much attention in this area [4-7]. In the case of microporous carbons, mass transfer limitations strongly influence diffusion of substrates toward active sites distributed inside pores as well as evacuation of products from the pore system. This obstacle can be overcome by using of carbon catalysts with well-ordered mesopore structure [8]. The ordered mesoporous carbons (OMC) are often prepared by the inverse nanoreplication of a silica hard template providing a tool for controlling uniform pore size and architecture in a produced carbon replica. The surface chemistry of carbon replica is mainly affected by a type of carbon precursor and synthesis conditions [9]. The CMK-type materials (e.g. CMK-1, CMK-3 and CMK-6, synthesized using of MCM-48, SBA-15 and SBA-16 silica templates, respectively) are the most important representatives of OMC [10-12].

The oxidative dehydrogenation of alkanes is one of the most promising reactions catalyzed by carbon materials. For example, the oxidative dehydrogenation of ethylbenzene (ODH) enables to produce styrene [7, 13, 14], which is an important monomer applied in the plastics and thermal insulation manufacturing. In contrast to the commercially used equilibrium-controlled dehydrogenation of ethylbenzene, ODH exhibits an exothermic heat effect and operates out of thermodynamic limitations (substantial conversions can be achieved even at low temperatures keeping high selectivity to the desirable product). Carbon materials, characterized by the presence of superficial carbonyl/quinone functional groups, are expected to be efficient catalysts of ODH, because the above-mentioned surface species are commonly identified as the active sites in this reaction [4, 15, 16]. Therefore, various carbon-based catalysts (e.g. soot, graphite, carbon nanofilaments [14], activated carbons [16, 17], multi-walled carbon nanotubes, onion-like carbons [18, 19], nanodiamonds [20]) were tested in

ODH. Among them, CMK-type materials showed a very attractive catalytic activity [8, 21-23].

Since diffusion limitations can play a significant role in the overall rate of heterogeneous reaction, it should be expected that the performance of CMK-type catalysts in ODH is influenced not only by a type and amount of active sites present on a surface, but also by a pore architecture of particular carbon replica. However, no clear evidences have been shown in the literature on these effects, especially because the pore structure of materials is so complicated that calculations of diffusion related parameters (e.g. tortuosity, Thiele modulus) is quite problematic. Furthermore, the process proceeds according to a very complex mechanism including partial oxidation of carbon catalyst by an oxidizing agent and a formation of carbonaceous deposit. Nevertheless, the role of diffusion limitations in the final performance of CMK-type catalysts seems to be interesting and should be clarified.

In this paper we present a comprehensive study of tailoring texture and surface chemistry of CMK-1 and CMK-3 carbon replicas by changing synthesis conditions, i.e. a kind of silica template and carbon precursor as well as carbonization temperature. The prepared carbon materials were tested in ODH. To the best of our knowledge, this is a first attempt on the comparison of catalytic activity of different carbon replicas synthesized by the same method. That allowed us to select samples with similar textural and chemical properties, but various in spatial structure (CMK-1 and CMK-3 exhibit regular and hexagonal symmetry, respectively) in order to investigate the extent of diffusion limitations (related to different tortuosity of the studied catalysts) during the catalytic reaction.

2. Experimental

2.1. Synthesis of CMK-1 and CMK-3 carbon replicas

Required MCM-48 and SBA-15 silica templates were synthesized using the methods described earlier [22, 23]. The carbon precursors were deposited in the pore system of mesoporous silicas by precipitation polycondensation of furfuryl alcohol (FA) or incipient wetness impregnation with sucrose. For the poly(furfuryl alcohol) (PFA)-derived replicas, the intended FA/MCM-48 and FA/SBA-15 mass ratios were equal to 1.25 and 2.00, respectively. The selected mass ratios were verified by low-temperature N_2 adsorption to be optimal for complete filling of silica pores. Consequently, the incomplete pore filling as well as deposition of additional amount of PFA on the external surface of SiO_2 were strongly limited. An amount of 3 g of silica template (dried initially at 120 °C for 1 h) was dispersed in a round-bottom flask (250 mL) containing a mixture of appropriate mass of FA (98 %, Aldrich) and water (the total mass of FA and water mixture was equal to 100 g). The flask was equipped with a reflux condenser, placed onto a magnetic stirrer and agitated (400 rpm) at room temperature for 30 min. Then, HCl (35-38 %, Chempur) was added as a polycondensation catalyst at the HCl/FA molar ratio of 6:1 and the temperature was raised to 100 °C. The obtained slurry was stirred at this temperature for 6 h. The resulting PFA/silica composite was filtered, washed with distilled water and dried at room temperature overnight.

For the sucrose-derived replicas, 1 g of silica template (dried initially at 120 °C for 1 h) was impregnated with a solution containing: (i) 2.87 g of water, 0.72 g of sucrose (POCH) and 0.08 g of sulfuric acid (95-97%, Sigma-Aldrich) in the case of MCM-48, or (ii) 3.37 g of water, 0.85 g of sucrose and 0.09 g of sulfuric acid in the

case of SBA-15. The obtained composites were placed in an oven at 100 °C for 6 h. Subsequently, the temperature was raised to 160 °C and the samples were kept at this temperature for the next 6 h. The procedure of impregnation and heating was repeated once, with a solution containing: (i) 1.78 g of water, 0.45 g of sucrose and 0.05 g of sulfuric acid for MCM-48, or (ii) 2.05 g of water, 0.51 g of sucrose and 0.06 g of sulfuric acid for SBA-15.

All obtained materials were carbonized in a tubular furnace at 650, 750, 850, 950 or 1050 °C for 4 h (with a heating rate of 1 °C/min) in an inert atmosphere (N_2). Finally, the silica templates were removed by a treatment with a 5 % HF solution at room temperature for 1 h. The produced carbon replicas were filtered, washed with distilled water and ethyl alcohol (96 %, Avantor) and dried at room temperature overnight. The procedure of silica dissolution was repeated once.

The CMK-1 and CMK-3 samples synthesized with sucrose (S) and PFA are denoted as *x*_CMK-1_S, *x*_CMK-1_PFA, *x*_CMK-3_S and *x*_CMK-3_PFA, respectively (where *x* is the carbonization temperature).

2.2. Characterization methods

Powder X-ray diffraction (XRD) patterns of synthesized carbon replicas were collected with a Bruker D2 Phaser instrument using Cu Kα radiation (λ= 1.54184 Å) and a LYNXEYE detector in the 2θ range from 0.5 to 8.0° with a step of 0.02° and 1 s counting time per the step.

Textural parameters were investigated on the basis of low-temperature nitrogen adsorption-desorption isotherms collected at -196 °C using two sorptometers, i.e. Micromeritics ASAP 2020 and a homemade fully automated equipment, designed and

constructed by the Advanced Materials Group (LMA), being commercialized as N_2GSorb-6 (Gas to Materials Technology). Prior to each measurement, a sample was degassed in vacuum (10^{-3} Pa) at 250 °C for 6 h. Specific surface areas and pore size distributions were calculated using the Brunauer–Emmett–Teller (BET) and Barrett-Joyner-Halenda (BJH) methods, respectively. Values of total pore volume (V_{total}) were obtained from amounts of nitrogen adsorbed at relative pressure of 0.97. Micropore volumes (V_{micro}) were determined using the Dubinin-Radushkevich equation, whereas mesopore volumes (V_{meso}) were calculated as differences between V_{total} and V_{micro}.

Temperature-programmed desorption (TPD) measurements were performed to determine a nature and total amount of oxygen-containing surface functionalities. The experiments were carried out by heating 100 mg of a sample placed in a U-shaped microreactor from ambient temperature up to 1000 °C (with a heating rate of 10 °C/min) under a helium flow (50 mL/min). Evolving CO and CO_2 were analyzed quantitatively with an Omnistar Balzer MSC200 quadrupole mass spectrometer after calibration based on decomposition of calcium oxalate ($CaC_2O_4 \cdot H_2O$). The deconvolution of CO profiles was performed by using the multiple Gaussian function with non-linear optimization procedure based on the Levenberg–Marquardt iteration algorithm.

Transmission electron spectroscopy (TEM) was used to visualize morphology of produced carbon replicas. The images were collected in a JOEL JEM-2010 microscope equipped with an Oxford Inca Energy TEM 100 detector and a Gatan Orius SC600 digital camera, operating at 200 kV. Prior to the experiments, the samples were deposited on a copper grid with a carbon film support.

2.3. Catalytic tests

The prepared CMK-1 and CMK-3 carbon replicas were tested as catalysts in the oxidative dehydrogenation of ethylbenzene (EB) to styrene in the presence of oxygen at the molar ratio of O_2:EB = 1:1. The reaction was carried out in a packed bed flow microreactor with 50 mg of a sample placed onto a quartz wool plug. The temperature was measured with a thermocouple, protected by a quartz capillary inserted directly into a catalyst bed. The gaseous reactants were fed through mass flow controllers (Brooks 4800) at a total flow rate of 50 mL/min (0.4 mL O_2 and 49.6 mL He). The EB vapor was introduced into the flow of O_2/He mixture by passing it through a glass saturator filled with liquid EB and kept at 25 °C. The products of the reaction were sampled with a pneumatic valve and transferred into a gas chromatograph system (Bruker 450-GC) via a heated line. The gas chromatograph was equipped with three packed columns (Porapak Q, Molecular Sieve 5A and Chromosorb W-HP) connected with two flame ionization detectors (one of them directly connected to a catalytic methanizer) and one thermal conductivity detector. Pictures of the system for catalytic tests and the quartz microreactor are presented in Fig. S1.

Prior to a catalytic run, a carbon replica was outgassed at 200 °C in flowing He (50 mL/min) for 30 min. Subsequently, the temperature was increased to 350 °C and dosing of reactants begun. After 15 minutes of time-on-stream (TOS), a first sample of outlet stream was injected to GC and the analysis started. The chromatographic analyses were performed in 42 min intervals with a total time of 7 h. The catalytic performance was evaluated in terms of the following parameters:

$$X_{EB} = ((F_{EB,0} - F_{EB}) / (F_{EB,0})) \times 100\%$$

$$Y_i = (F_i / F_{EB,0}) \times 100\%$$

$S_i = (Y_i / X_{EB}) \times 100\%$

where X_{EB} – conversion of EB, $F_{EB,0}$ and F_{EB} – molar flow rate of EB in the inlet and outlet streams, Y_i – yield of *i* product, F_i – molar flow rate of EB transformed into *i* product, and S_i – selectivity of *i* product.

3. Results and discussion

3.1. Structural properties of carbon replicas

In order to verify structural properties of CMK-1 and CMK-3 carbon replicas, the low-angle powder X-ray diffraction measurements were performed. In the XRD patterns of all CMK-1 replicas synthesized with sucrose and PFA precursors (Fig. 1A and 1B) two distinct peaks, indexed as the (110) and (211) reflections in $I4_132$ cubic space group, are observed [24, 25]. Nevertheless, the structure of CMK-1 carbon is influenced by the type of carbon precursor used. For the PFA-based samples both diffraction lines are relatively sharp and well visible, whereas for the sucrose-derived replicas they are much wider and less intense. This suggests that using the precipitation polycondensation of FA the pore system of MCM-48 is filled more efficiently and the material retains more long-range ordering compared to impregnation with the sucrose solution. The calculated values of lattice parameter a_0 and interplanar spacing d_{110} are summarized in Table 1. The determined structural parameters are similar within the whole range of carbonization temperatures for the sucrose-based replicas (a_0 = 6.8 nm and d_{110} = 4.8 nm). In the case of the PFA-based materials, these values are slightly higher after carbonization at 650 °C (a_0 = 7.2 nm and d_{110} = 5.1 nm) and decrease with raising carbonization temperatures to the level found for the CMK-1_S series. It should

however be noticed that even for the carbon materials thermally treated at temperature as high as 1050 °C, the structure of replica is well preserved.

The XRD patterns of the CMK-3 replicas (Fig. 1C and 1D) exhibit three individual peaks, which can be indexed as the (100), (110) and (200) reflections typical of hexagonal *P6mm* space group [26]. For both series of CMK-3, similar effects as for CMK-1 are clearly observed, i.e. (i) carbonization temperature does not influence the specific structure, because all XRD patterns look comparable; (ii) the type of carbon precursor alters the structure uniformity. For all CMK-3_PFA replicas diffraction lines are much narrower and more visible than for the sucrose-derived CMK-3 samples. Additionally, the values of a_0 (= 8.7 nm) and d_{100} (= 7.6 nm) are constant for the CMK-3_S series, but become higher for the CMK-3_PFA samples especially those carbonized at lower temperatures (a_0 = 9.4 nm and d_{100} = 8.1 nm) (Table 1).

It can therefore be concluded that penetration of pores of silica template by the carbon precursor is better during the precipitation polycondensation of FA than for impregnation with sugar also in the case of hexagonal SBA-15. It was shown that during the initial step of precipitation polycondensation, molecules of FA are easily chemisorbed on silanol groups present on the silica surface [27]. Consequently, these adsorbed species can take part in polycondensation after an addition of HCl resulting in a growth of polymer chain from the wall to the center of pore. When the process is finalized, the whole mesopores are almost perfectly filled with the PFA chains, which are additionally chemically bonded to the silica walls (Fig. 2A).

In the case of impregnation with the sucrose solution, the interaction of sugar molecules with the silanol groups is weaker. Thus, during evaporation of the solvent and partial condensation of the carbon precursor, the sucrose-derived polymer rods are

condensed in the centers of mesopores and voids close to the silica walls are formed, even after the second impregnation (Fig. 2B). The described processes are similar for both silica templates. However, the presence of micropores in the SBA-15 silica walls plays an additional role in stabilization of carbon replica structure. It is most likely that the carbon spacers distributed between the carbon rods are more perfectly formed for sucrose-derived CMK-3 compared to PFA-based CMK-3, because in the former case no polycondensation initiator has to diffuse inside the pore spacers and micropores are filled more capably with the condensed carbon precursor. Concluding, PFA, which entirely fills the mesopore system, protects efficiently a SBA-15/PFA composite against shrinkage during carbonization, but simultaneously forms less stable carbon spacers providing a more packed CMK-3 structure than that observed for the sucrose-derived replicas (cf. Fig. 2A and 2B). In the case of the sucrose-based CMK-3, the voids formed during heating between the carbon precursor and silica walls result in greater shrinkage of the entire structure, even though the carbon spacers in micropores are better shaped. These effects are confirmed by the lower a_0 and d_{100} parameters for the CMK-3_S materials compared to the CMK-3_PFA ones. Moreover, the pore sizes (Table 1) are wider for CMK-3_S (~ 3.8 nm) than CMK-3_PFA (~ 3.5 nm) despite the greater overall shrinkage, therefore the sucrose derived carbon rods must have smaller diameter to match the structural parameters, i.e. a_0, d_{100} and pore diameter. This relationship is illustrated in Fig. 2. The shrinkage of these kind of nanostructures is a well-known fact, but the influence of the carbon precursor on this phenomenon is quite interesting [26, 28]. Furthermore, the presented discussion is in agreement with the structural parameters obtained for CMK-1, since there is no influence of micropores connectors in the case of MCM-48 silica template. Because of that fact, the effect of lower diameter

of carbon rods originated from sucrose is compensated with a greater shrinkage and as a result, the mesopore diameter is similar for both CMK-1_S and CMK-1_PFA replicas (ca. 3.6 nm). All calculated parameters are comparable with those reported elsewhere for CMK-1 and CMK-3, however the number of papers regarding furfuryl alcohol as a carbon precursor is rather limited [21, 26, 29-31]. Moreover, the method of precipitation polycondensation of FA is quite unique [22, 23].

To investigate deeper morphology of the studied replicas, the TEM micrographs were taken. The images recorded for four samples thermally treated at 850 °C are depicted in Fig. 3. The presented results confirm that for both CMK-1 and CMK-3 carbon replicas, the nanoreplication process resulted in the formation of expected spatial structure. Nevertheless, it can be found that the samples produced using the sucrose and PFA precursors differ in terms of structure uniformity. The arrangement and regularity of carbon rods are significantly higher for the materials derived from PFA, as previously concluded from XRD. This effect is observed both for CMK-1 (Fig. 3A and 3B) as well as CMK-3 imaged in direction perpendicular (Fig. 3C and 3D) and parallel (Fig. 3C’ and 3D’) to the pores. The recorded TEM micrographs enabled us to determine mean carbon rod diameters, which is 6.4 and 6.9 nm for 850_CMK-3_S and 850_CMK-3_PFA, respectively. The differences between the a_0 parameters and estimated diameters of carbon rod in both cases are equal to 2.3 nm that can be interpreted as the distance between two adjacent carbon rods. The value obtained for 850_CMK-3_PFA is similar to the size of mesopores in the SBA-15 template, confirming limited shrinkage of PFA during carbonization discussed previously based on the XRD results.

3.2. Textural properties of carbon replicas

The textural parameters of the synthesized materials were investigated by low-temperature N_2 sorption measurements. In the case of CMK-1 carbon replicas, the recorded isotherms (Fig. 4) can be assigned to the type IVa according to IUPAC, which confirm the micro-mesoporous character of these materials [32]. Moreover, the hysteresis loop of type H4, typical of CMK-1 carbon replicas [25], is distinguished for all samples. The synthesized CMK-1 materials exhibit relatively high and comparable specific surface areas, i.e. 1523-1671 m^2/g (PFA-based samples) and 1494-1588 m^2/g (sucrose-based samples). Only slight decrease in these values is observed with increasing carbonization temperature. The comparable total pore volume of 0.9-1.0 cm^3/g for all CMK-1 samples is also noticed. A substantial contribution of V_{meso} in the total pore volume (~ 50 %) confirms the important role of mesoporosity. The carbon precursor does not influence significantly the textural parameters of CMK-1 and only slight differences in specific surface area are observed between PFA- and sucrose-derived replicas. It is noteworthy that spatial system of pores in CMK-1 is regular, but quite complex. This material is not an exact replica of gyroid-type MCM-48 structure, since transition into another $I4_132$ space group occurs during replication [24]. The micro-mesoporous type IVa isotherms of both CMK-3 series (Fig. 5A and 5B) show small hysteresis loops (type H4) in the range of p/p_0 = 0.4-0.6, which are typical of CMK-3 mesoporous carbons [11].

As discussed for the CMK-1 samples, the carbonization temperature has an insignificant effect on the textural parameters of the CMK-3 replicas. Nevertheless, the textural parameters of CMK-3 materials obtained using different carbon precursors vary considerably, in contrast to CMK-1. The sucrose-derived CMK-3 catalysts exhibit

specific surface area of 1560-1630 m^2/g, similar to those described earlier in the literature [11, 33], and are higher than the samples based on PFA (1020-1190 m^2/g). The same trend is found for total pore volume, i.e. ~ 1.5 cm^3/g and ~ 1.0 cm^3/g for the sucrose- and PFA-derived materials, respectively. The observed differences can be explained by two possible mechanisms. The most prominent is related to the nature of carbon precursor. Simply, thermal decomposition of sucrose results in the formation of more microporous material than in the case of PFA. This assumption is confirmed by the greater amount of nitrogen adsorbed in the micropore-related region of isotherm ($p/p_0 < 0.01$). However, the differences are also distinct in the mesopore range (p/p_0 = 0.50-0.95), where the volume adsorbed increases consistently for the CMK-3_S series in contrast to CMK-3_PFA demonstrating plateau there. Węgrzyniak et al. also reported substantial differences in textural parameters of sucrose- and FA-derived CMK-3 (both replicas were synthesized by impregnation) and explained the observed effects by various behavior of both carbon precursors during thermal decomposition [34].

Another reason of variations in the textural parameters of CMK-3 series is related to the above-described presence of microporous connectors in the SBA-15 silica template and the nature of silica-carbon precursor interaction. Namely, the PFA-based CMK-3 structure is more packed due to weaker PFA spacers, which can crush upon heating, resulting in limited total pore volume. Even though the sucrose-derived replicas undergo the greater temperature induced shrinkage of entire composite, the resulting carbon structure reveals the higher values of textural parameters, including higher mesopore diameters (cf. Table 1).

The above-discussed mechanisms are not valid in the case of CMK-1, because of similar textural parameters are achieved for both PFA- and sucrose-based series. It is

most likely that development of additional porosity in CMK-1_S is blocked in gyroid-type pore system by diffusion limitations in the transport of gaseous decomposition products - diameters of mesopores in MCM-48 are additionally more than two times lower than in SBA-15 (cf. Table 1). Furthermore, XRD results show that no clear differences are observed in shrinkage for the MCM-48/carbon precursor composites filled with sucrose and PFA.

3.3. Surface composition of carbon replicas

The type and amount of functional groups formed on the entire catalyst surface were determined by TPD. Herein, the discussion is focused on carbonyl/quinone functionalities, since they are usually considered as active sites in ODH [4, 13, 15, 16, 35]. To estimate the content of C=O functional groups, the complete deconvolution and peak area integration were performed assuming decomposition of carbonyls/quinones into CO (mass line m/z = 28) with the highest intensity in the temperature range of 775-825 °C [4, 15, 36-39]. The recorded TPD profiles are presented in Fig. 6, whereas the results of quantitative analysis are summarized in Table 1.

It is evident that the overall amount of carbonyl/quinone functionalities is higher for the sucrose-derived samples. This effect can be explained by a lower number of oxygen atoms in FA precursor compared to sucrose (disaccharide), which partially remain on the surface after carbonization. Furthermore, the carbonization temperature alters the surface composition of both CMK-1 and CMK-3 carbon replicas, i.e. decreasing amount of C=O functionalities is observed. The highest concentration of these species is found for the samples carbonized at low temperatures – 650 °C (for CMK-3) and 750 °C (for CMK-1). These variations can be affected by associated

changes in the specific surface area of the material. However, the percentage decline of surface area for all carbon replica series (shown in Fig. 7) varies in the range from 4.5 % (for CMK-3_S) to 14.2 % (for CMK-3_PFA), and the surface concentrations of carbonyl/quinone groups differ much more, i.e. 37 % and 67 %, for CMK-1_S and CMK-3_S series, respectively. This comparison suggests that thermal-induced variations in the superficial atomic structure have much higher contribution in the TPD results than those related to the surface area. At higher temperatures, the rearrangement toward the graphitic structure is more intense, thus lower amounts of oxygen atoms remain on the surface in the form of oxygen functionalities. Accordingly, at lower temperatures, it is harder to remove non-carbonaceous atoms (like oxygen) and their concentration on the surface is distinctly higher. Moreover, the correlations depicted in Fig. 7 reveal that the CMK-1 samples are relatively more resistant to the decomposition of carbonyl/quinone surface species with increasing carbonization temperature than CMK-3.

3.4. Catalytic activity of carbon replicas in oxidative dehydrogenation of ethylbenzene

3.4.1. Effect of carbonization temperature and carbon precursor

The catalytic activity of the produced replicas was discussed in terms of conversion of EB and selectivity to styrene. The initial period of 15 min. of TOS was arbitrarily selected to represent steady state in the studied system at an insignificantly modified catalyst surface. In Fig. 8A and 8B the initial conversions of EB is presented for all CMK-1 and CMK-3 catalysts, respectively. As can be seen, the best catalytic performance among the CMK-1 replicas is achieved over the materials carbonized at

750 °C, i.e. 38.3 % and 30.3 % for 750_CMK-1_S and 750_CMK-1_PFA, respectively. A further increase in the carbonization temperature results in a gradual decrease in the catalytic activity, to 26.5 % and 19.6 % for 1050_CMK-1_S and 1050_CMK-1_PFA, respectively. The similar effects are found for the CMK-3 replicas, however in this case the highest EB conversion is noted for the catalysts carbonized at 650 °C. Interestingly, the catalytic activity of 750_CMK-3_S and 750_CMK-3_PFA decreases only slightly. The type of carbon precursor does not change the effect of continuous decrease of catalytic activity, neither for CMK-1 nor CMK-3 replicas. However, the EB conversions are generally lower for all samples based on the PFA carbon precursor in comparison to their sucrose-based counterparts. In order to investigate the effect of declining catalytic activity with increasing carbonization temperature, the surface concentration of carbonyl/quinone groups was compared with the initial EB conversion (Fig. 9A and 9B). Clear correlations for both sucrose- and PFA-based replicas are seen within the whole range of carbonization temperatures, which confirm previous findings for other nanocarbons [40]. The presented results are consistent with the commonly accepted ODH mechanism, which involves a redox cycle whereby an EB molecule reacts with two adjacent carbonyl/quinone groups and produces a styrene molecule. Finally, the formed hydroquinone groups are reoxidized by gaseous oxygen with H_2O evolution [4, 13-16, 35, 41-43].

The slope of linear fit for the CMK-1 samples is larger than for the CMK-3 ones, regardless of the type of carbon precursor. It should therefore be concluded that the catalytic activity of CMK-1 is more sensitive to the C=O surface concentration compared to CMK-3. In other words, the slighter modification of surface chemistry is required to change the initial catalytic activity of CMK-1.

Considering the selectivity to styrene, presented in Fig. 8C and 8D, more than 95% of EB is converted to the desirable product over all samples. Minor differences between the catalysts synthesized using both carbon precursors are realized, with a superior effect noticed for the PFA-based materials. The most important by-product formed in ODH is CO_2, since the selectivity to CO, benzene and toluene is lower than 1 % over all samples.

Gradual clogging of pores by carbon deposit, manifested by decreasing specific surface area and total pore volume, is observed in N_2 adsorption isotherms for samples collected at different stages of the reaction, i.e. at different time on stream (15, 60, 240, 390 and 780 min). The results for 850_CMK-1_PFA and 850_CMK-3_PFA, chosen as representative samples, are demonstrated in Fig. 10A and 10B. The formation of carbon deposit begins to be suppressed after 4 h of reaction time. The observed consecutive changes in the catalyst surface influence the long term catalytic performance. The conversion of EB and selectivity to styrene versus TOS are presented in Fig. S2 for the most active samples from each series. As can be seen, the EB conversion decreases gradually for all samples, reaching a plateau after ca. 6 h of TOS. On the other hand, the selectivity to styrene is kept at relatively high level during the whole catalytic run. It is most likely that aromatic hydrocarbons, especially styrene, modify the surface of carbon catalyst blocking in a consequence the pores. As a result, the surface and texture of catalyst are completely different after 6 h TOS compared to the fresh material.

3.4.2. Effect of pore structure

The relationship between catalytic activity and surface composition reveals that the CMK-1 samples are more active in ODH than the CMK-3 ones, despite the lower

concentration of surface carbonyl/quinone functionalities. The differences in the pore architecture between CMK-1 and CMK-3 might play a significant role in the observed phenomenon. To investigate the influence of structural features on the catalytic activity, two samples synthesized with the same carbon precursor (sucrose) and presenting comparable V_{total}, S_{BET} and carbonyl/quinone surface concentration were chosen, i.e. 650_CMK-1_S and 950_CMK-3_S. These samples exhibit the S_{BET} = 1546 m^2/g and 1559 m^2/g, as well as C=O surface concentration equal to 0.17 C=O/nm^2 and 0.16 C=O/nm^2, respectively. The different carbonization temperatures for these samples do not play a significant role, because the textural parameters are not influenced by this factor within the series. Furthermore, graphitization is negligible in both cases. Taking into account the foregoing similarities as well as postulated mechanism of ODH, the chemical vicinity on the surface of both carbon replica is reasonably alike for the EB molecules. Because of that fact, only pore structure remains an important factor diversifying these materials. Nonetheless, for the 650_CMK-1_S and 950_CMK-3_S replicas the initial EB conversion is 34.2 % and 21.6 %, respectively. The higher slope for the CMK-1 samples in Fig. 9A and 9B indicates that the surface functional groups are utilized more efficiently than for the CMK-3 samples. We explain this fact by an easier accessibility of active sites on the CMK-1 surface for the reactants as well as an easier evacuation of styrene from the pore system. This supposition is supported by comparing the activity parameter *a* [$\mu mol \cdot g_{cat}^{-1} \cdot s^{-1}$]:

$$a = (X_{EB} \cdot F_{EB,0}) / W$$

where: X_{EB} – EB conversion, $F_{EB,0}$ – molar flow rate of EB in the inlet stream, W – initial catalyst mass. For 650_CMK-1_S the *a* parameter is equal to 1.78, whereas for

950_CMK-3_S - 1.11. The former value is also higher than that described previously for activated carbon (1.47) [16] and carbon nanotubes (0.80-1.12) [19].

The differences in the catalytic activity of both selected carbon materials with comparable physical and chemical properties, but different 3D structure, may be considered as adequate premises to formulate hypothesis on the role of diffusion limitations. The lack of hard evidence in the form of pure mathematical calculations does not have to be disqualifying. At first glance, the quite complicated architecture of CMK-1 should be detrimental for the catalytic process, since the tortuosity of this material might be greater (many possible pathways of molecules migration). Nevertheless, it is most likely that the complicated, but regular pore structure of CMK-1 carbon replica favor reactants and products diffusion compared to the hexagonal pore arrangement in the CMK-3 replica, which is rather contradictory finding. A reasonable explanation of this fact may be that CMK-3 possesses relatively long pores, in which migration of molecules is straitened in perpendicular direction between consecutive hexagonally-arranged carbon rods. This parameter can be important from the point of view of distribution of particles in a catalyst bed. The spatial arrangement of the catalyst particles in a reactor is stochastic, thus the catalytic performance of CMK-3 can be sensitive to the orientation of these particles towards the direction of gas flow. In this regard, the structure of CMK-1 is more resistant to this parameter, since it exhibits the regular symmetry.

4. Conclusions

Mesoporous ordered carbons with different pore architectures (regular and hexagonal mesopore arrangement) were synthesized by nanoreplication of silica

templates (MCM-48 and SBA-15) using sucrose or PFA as the carbon precursor. The deposition of PFA by the precipitation polycondensation resulted in more perfect pore filling, because of the precursor molecules were initially chemisorbed on the silica walls and the formed polymer chains grew towards the centers of pores blocking them entirely. After the solvent removal, the mesopores remained filled continuously in contrast to sucrose, which formed voids between the condensed carbon precursor and silica walls. The pore filling influenced the behavior of the carbon precursor/silica composite during carbonization. Significantly larger shrinkage took place in the case of sucrose-derived materials.

On the other hand, the carbon spacers present in the CMK-3 structure were more stable after the deposition of disaccharide, which did not demand the addition of initiator. That resulted in the formation of wider mesopores and more expanded surface areas in the final replicas. Furthermore, during decomposition the carbon precursor generated microporosity, which accompanied mesoporosity obtained by the replication effect. The higher micropore volume was found for the sucrose-derived CMK-3 materials compared to the PFA-derived ones. In the case of the CMK-1 samples diffusion limitations caused that this effect was less distinct.

The decomposition of sucrose resulted in higher amounts of surface C=O functionalities as well. Nevertheless, the concentration of these species was strongly influenced by the carbonization temperature. It was found that the content of C=O functional groups was straightly correlated to the initial activity of the produced replicas in ODH, confirming the redox mechanism of this reaction. Additionally, the CMK-1 carbon replicas appeared to be more active compared to the analogous CMK-3 catalysts despite to the lower concentration of C=O species considered as the active sites. The

observed phenomenon was related to the pore architecture. The regular pore arrangement in CMK-1 obviously favored the diffusion of reactant molecules during the catalytic process.

Acknowledgements

This work was supported by the Polish National Science Centre (grant no. 2013/09/B/ST5/03419), MINECO (Project MAT2016-80285-p) and Generalitat Valenciana (PROMETEOII/2014/004). The research was carried out with the equipment purchased thanks to the financial support of the European Regional Development Fund in the framework of the Polish Innovation Economy Operational Program (contract no. POIG.02.01.00-12-023/08). Sebastian Jarczewski received funds from the Polish National Science Centre in the form of a doctoral scholarship (grant no. 2016/20/T/ST5/00256).

References

[1] P.T. Anastas, J.C. Warner, Green Chemistry: Theory and Practice, Oxford University Press, New York, 1998, p.30.

[2] X. Liu, L. Dai, Nat. Rev. Mater. 1(16064) (2010) 1-12.

[3] D.S. Su, J. Zhang, B. Frank, A. Thomas, X. Wang, J. Parankowitsh, R. Schlögl, ChemSusChem 3 (2010) 169-180.

[4] P. Serp, J.L. Figueiredo, Carbon materials for catalysis, Wiley, New Jersey, 2009, pp. 75-78.

[5] L. Liu, Y-P. Zhu, M. Su, Z-Y. Yuan, ChemCatChem 7 (2015) 2765-2787.

[6] F. Rodríguez-Reinoso, Carbon 36(3) (1998) 159-175.

[7] D. Chen, A. Holmen, Z. Sui, X. Zhou, Chin. J. Catal. 35 (2014) 824-841.

[8] D.S. Su, J.J. Delgado, X. Liu, D. Wang, R. Schlögl, L. Wang, Z. Zhang, Z. Shan, F-S. Xiao, Chem. Asian. J. 4 (2009) 1108-1113.

[9] M. Enterría, J.L. Figueiredo, Carbon 108 (2016) 79-102.

[10] R. Ryoo, S.H. Joo, S. Jun, J. Phys. Chem. B 103 (1999) 7743-7746.

[11] R. Ryoo, S.H. Joo, M. Kruk, M. Jaroniec, Adv. Mater. 13(9) (2001) 677-681

[12] W. Guo, F. Su, X.S. Zhao, Carbon 43 (2005) 2397-2429.

[13] F. Cavani, F. Trifirò, Appl. Catal. A 133 (1995) 219-239.

[14] G. Mestl, N.I. Maksimova, N. Keller, V.V. Roddatis, R. Schlögl, Angew. Chem. Int. Ed. 40 (2001) 2066-2068.

[15] J.L. Figueiredo, M.F.R. Pereira, Catal. Today 150 (2010) 2-7.

[16] M.F.R. Pereira, J.J.M. Órfão, J.L. Figueiredo, Appl. Catal. A 184 (1999) 153-160.

[17] V. Zarubina, H. Talebi, C. Nederlof, F. Kapteijn, M. Makkee, I. Melián-Cabrera, Carbon 77 (2014) 329-340.

[18] D.S. Su, N. Maksimova, J.J. Delgado, N. Keller, B. Mestl, M.J. Ledoux, R. Schlögl, Catal. Today 102-103 (2005) 110-114.

[19] M.F.R. Pereira, J.L. Figueiredo, J.J.M. Órfão, P. Serp, P. Kalck, Y. Kihn, Carbon 42 (2004) 2807-2813.

[20] D. Su, N.I. Maksimova, G. Mestl, V.L. Kuznetsov, V. Keller, R. Schlögl, N. Keller, Carbon 45 (2007) 2145-2151.

[21] P. Janus, R. Janus, P. Kuśtrowski, S. Jarczewski, A. Wach, A.M. Silvestre-Albero, F. Rodríguez-Reinoso, Catal. Today 235 (2014) 201-209.

[22] S. Jarczewski, M. Drozdek, A. Wach, B. Dudek, P. Kuśtrowski, M.E. Casco, F. Rodríguez-Reinoso, Catal. Lett. 146 (2016) 1231-1241.

[23] P. Niebrzydowska, R. Janus, P. Kuśtrowski, S. Jarczewski, A. Wach, A.M. Silvestre-Albero, F. Rodríguez-Reinoso, Carbon 64 (2013) 252-261.

[24] M. Kaneda, T. Tsubakiyama, A. Carlsson, Y. Sakamoto, T. Ohsuna, O. Terasaki, S.H. Joo, R. Ryoo, J. Phys. Chem. B 106 (2002) 1256-1266.

[25] M. Kruk, M. Jaroniec, R. Ryoo, S.H. Joo, J. Phys. Chem. B 104(33) (2000) 7960-7968.

[26] M. Kang, S.H. Yi, H.I. Lee, J.E. Yie, J.M. Kim, Chem. Commun. 8 (2002) 1944-1945.

[27] K. Machowski, P. Kuśtrowski, B. Dudek, M. Michalik, Mater. Chem. Phys. 165 (2015) 253-260.

[28] A.H. Lu, W. Schmidt, A. Taguchi, B. Spliethoff, B. Tesche, F. Schüth, Angew. Chem. Int. Ed. 41 (2002) 3489-3492.

[29] M. Leżańska, P. Pietrzyk, A. Dudek, J. Włoch, Mater. Chem. Phys. 149-150 (2015) 539-552.

[30] M.A. Kiani, H. Khani, N. Mohhamadi, J. Solid State Electrochem. 18 (2014) 1117-1125.

[31] R. Janus, P. Natkański, M. Wądrzyk, B. Dudek, M. Gajewska, P. Kuśtrowski, Mater. Today Commun. 13 (2017) 6-22.

[32] M. Thommes, K. Kaneko, A.V. Neimark, J.P. Olivier, F. Rodriguez-Reinoso, J. Rouquerol, K.S.W. Sing, Pure Appl. Chem. 87(9-10) (2015) 1051-1069.

[33] S.H. Joo, R. Ryoo, M. Kruk, M. Jaroniec, J. Phys. Chem. B 106 (2002) 4640-4646.

[34] A. Węgrzyniak, S. Jarczewski, P. Kuśtrowski, P. Michorczyk, J. Porous Mater. (2017) 1-10.

[35] M.F.R. Pereira, J.J.M. Órfão, J.L. Figueiredo, Appl. Catal. A 218 (2001) 307-318.

[36] J.L. Figueiredo, M.F.R. Pereira, M.M.A. Freitas, J.J.M. Órfão, Carbon 37 (1999) 1379-1389.

[37] G.S. Szymański, Z. Karpiński, S. Biniak, A. Świątkowski, Carbon 40 (2002) 2627-2639.

[38] J-H. Zhou, Z-J. Sui, J. Zhu, P. Li, D. Chen, Y-C. Dai, W-K. Yuan, Carbon 45 (2007) 785-796.

[39] M.J. Lázaro, L. Calvillo, E.G. Bordejé, R. Moliner, R. Juan, C.R. Ruiz, Microporous Mesoporous Mater. 103 (2007) 158-165.

[40] W. Qi, W. Liu, B. Zhang, X. Gu, X. Guo, D. Su, Angew. Chem. Int. Ed. 52 (2013) 14224-14228.

[41] G. Emig, H. Hofmann, J. Catal. 84 (1983) 15-26.

[42] J.A. Maciá-Agulló, D. Cazorla-Amorós, A. Linares-Solano, U. Wild, D.S. Su, R. Schlögl, Catal. Today 102-103 (2005) 248-253.

[43] M.F.R. Pereira, J.J.M. Órfão, J.L. Figueiredo, Appl. Catal. A 196 (2000) 43-54.

Table 1. Structural, textural and surface properties of CMK-1 and CMK-3 carbon replicas.

	Lattice parameter a_0 [nm]	d_{hkl} [nm]	S_{BET} [m^2/g]	V_{total} [cm^3/g]	V_{micro} [cm^3/g]	V_{meso} [cm^3/g]	Mesopore diameter[d] [nm]	Carbonyl / quinone groups[e] [μmol/g]
MCM-48	7.8	3.2[a]	1202	0.84	0.38	0.46	2.5	-
SBA-15	10.3	8.9[b]	889	0.97	0.33	0.61	6.8	-
650_CMK-1_S	6.8	4.8[c]	1546	1.02	0.47	0.55	3.6	427
750_CMK-1_S	6.8	4.8[c]	1576	1.04	0.49	0.55	3.6	497
850_CMK-1_S	6.8	4.8[c]	1528	0.99	0.47	0.52	3.6	449
950_CMK-1_S	6.8	4.8[c]	1588	1.02	0.49	0.54	3.6	361
1050_CMK-1_S	6.8	4.8[c]	1494	0.94	0.47	0.47	3.6	297
650_CMK-1_PFA	7.2	5.1[c]	1671	1.04	0.46	0.58	3.6	259
750_CMK-1_PFA	6.9	4.9[c]	1700	1.03	0.49	0.54	3.6	318
850_CMK-1_PFA	6.9	4.9[c]	1629	0.96	0.45	0.47	3.6	233
950_CMK-1_PFA	6.8	4.8[c]	1625	0.97	0.48	0.49	3.6	206
1050_CMK-1_PFA	6.8	4.8[c]	1523	0.91	0.57	0.27	3.6	160
650_CMK-3_S	8.7	7.6[b]	1630	1.43	0.56	0.88	3.6	1108
750_CMK-3_S	8.7	7.6[b]	1591	1.48	0.54	0.93	3.6	749
850_CMK-3_S	8.7	7.6[b]	1599	1.54	0.56	0.98	3.8	629
950_CMK-3_S	8.7	7.6[b]	1559	1.50	0.54	0.96	3.8	427
1050_CMK-3_S	8.7	7.6[b]	1557	1.48	0.54	0.94	3.8	349
650_CMK-3_PFA	9.4	8.1[b]	1187	0.99	0.39	0.60	3.3	521
750_CMK-3_PFA	9.4	8.1[b]	1157	0.98	0.41	0.57	3.5	454
850_CMK-3_PFA	9.2	8.0[b]	1128	0.97	0.40	0.57	3.5	379
950_CMK-3_PFA	9.2	8.0[b]	1078	0.95	0.37	0.58	3.5	199
1050_CMK-3_PFA	9.1	7.8[b]	1019	0.90	0.36	0.54	3.4	153

a – d_{211}; *b* – d_{100}; *c* – d_{110}; *d* – BJH; *e* – TPD.

Figure captions

Fig. 1. Low-angle X-ray powder diffraction patterns collected for the CMK-1_S (A), CMK-1_PFA (B), CMK-3_S (C) and CMK-3_PFA (D) replicas carbonized at various temperatures.

Fig. 2. Postulated carbon precursor interaction with silica template walls for PFA (A) and sucrose (B) in the process of nanoreplication.

Fig. 3. TEM micrographs taken for 850_CMK-1_S (A), 850_CMK-1_PFA (B), 850_CMK-3_S perpendicular (C) and parallel (C') to the pores, 850_CMK-3_PFA perpendicular (D) and parallel (D') to the pores.

Fig. 4. Low-temperature N_2 sorption isotherms of the CMK-1_S (A) and CMK-1_PFA (B) carbon replicas carbonized at different temperatures. Isotherms were equally shifted (with a step of 100 cm^3/g) to make graph more readable.

Fig. 5. Low-temperature N_2 sorption isotherms of the CMK-3_S (A) and CMK-3_PFA (B) carbon replicas carbonized at different temperatures. Isotherms were equally shifted (with a step of 100 cm^3/g) to make graph more readable.

Fig. 6. TPD profiles of CO evolution for the CMK-1_S (A), CMK-1_PFA (B), CMK-3_S (C) and CMK-3_PFA (D) replica series carbonized at different temperatures.

Fig. 7. Induced decline (%) in the S_{BET} and carbonyl/quinone surface concentration for all carbon replica series at a given carbonization temperature.

Fig. 8. Initial conversion of EB and selectivity to styrene for CMK-1 (A, C) and CMK-3 (B, D) carbon replicas.

Fig. 9. Relation between initial conversion and surface concentration of carbonyl/quinone functional groups for sucrose derived (A) and PFA-derived (B) carbon replicas.

Fig. 10. Changes of S_{BET} and V_{total} for 850_CMK-1_PFA (A) and 850_CMK-3_PFA (B) with increasing time on stream.

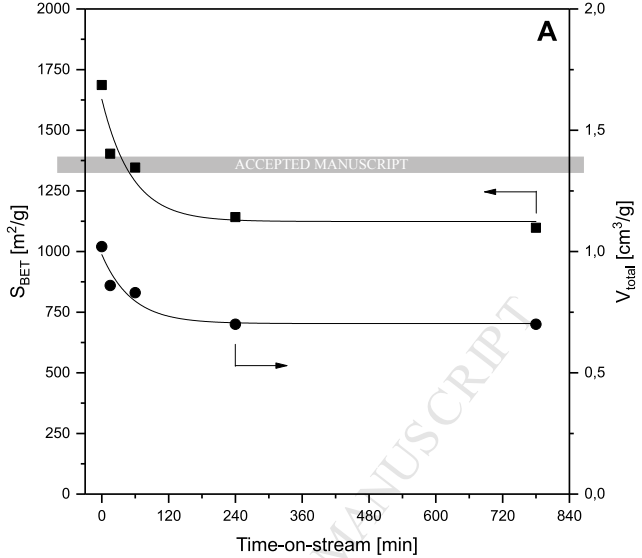

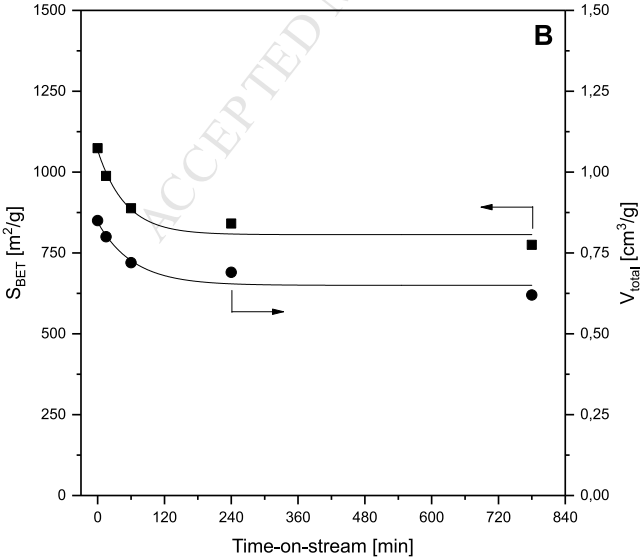

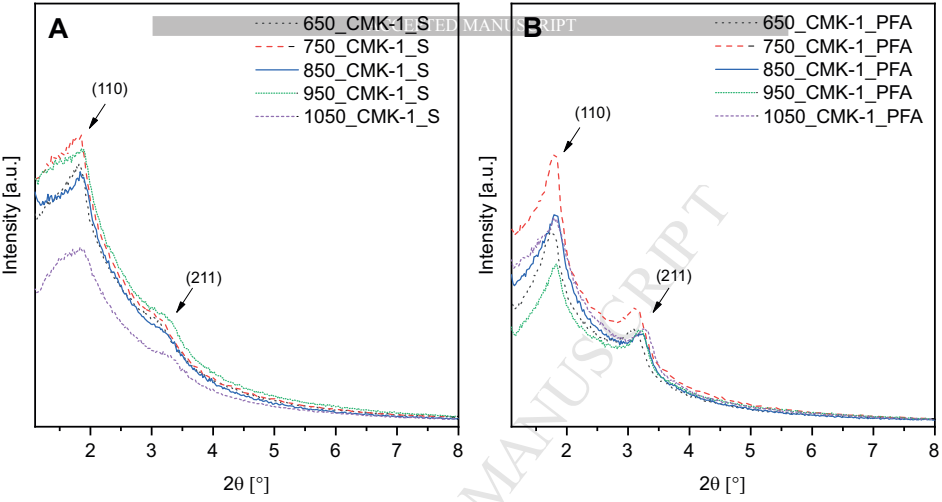

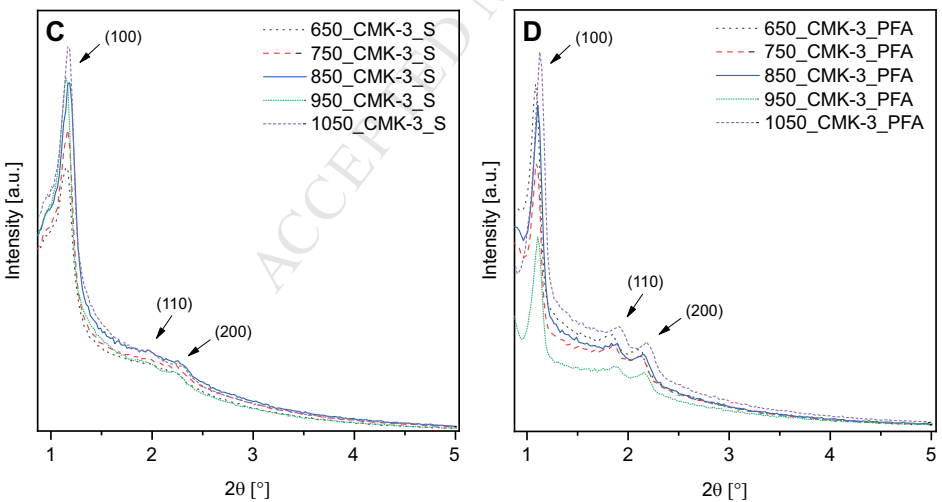

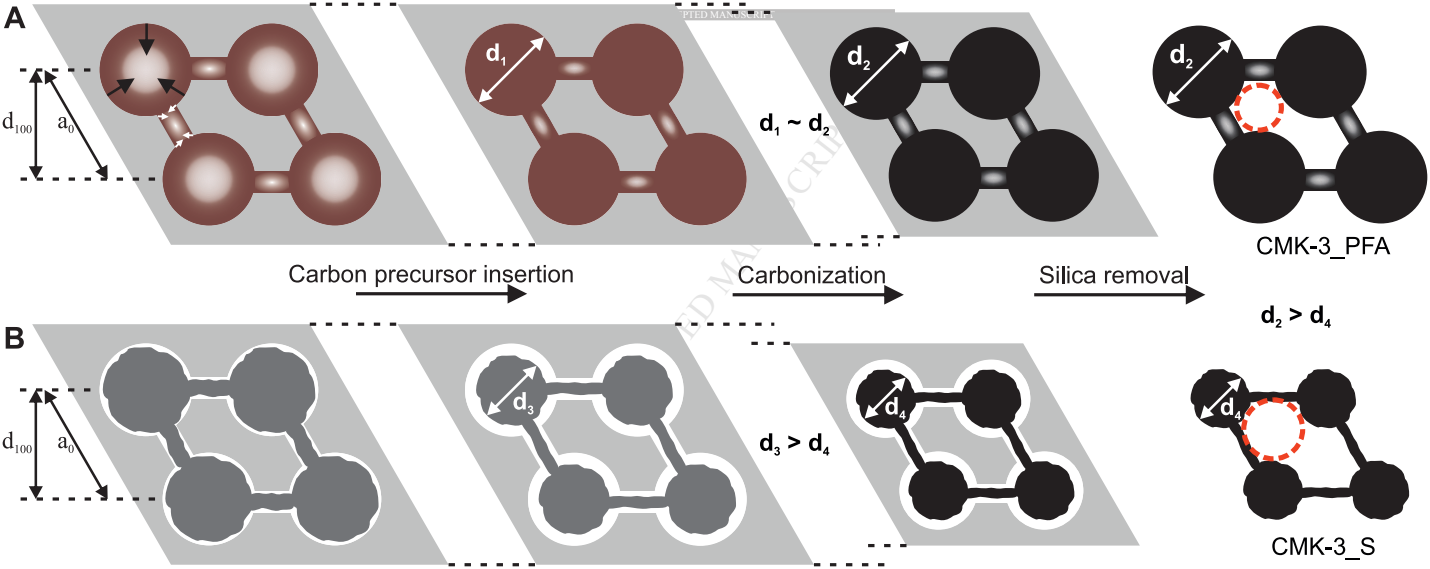
A
d100
a0
d1
d1 ~ d2
d2
d2
CMK-3_PFA
Carbon precursor insertion
Carbonization
Silica removal
d2 > d4
B
d100
a0
d3
d3 > d4
d4
d4
CMK-3_S

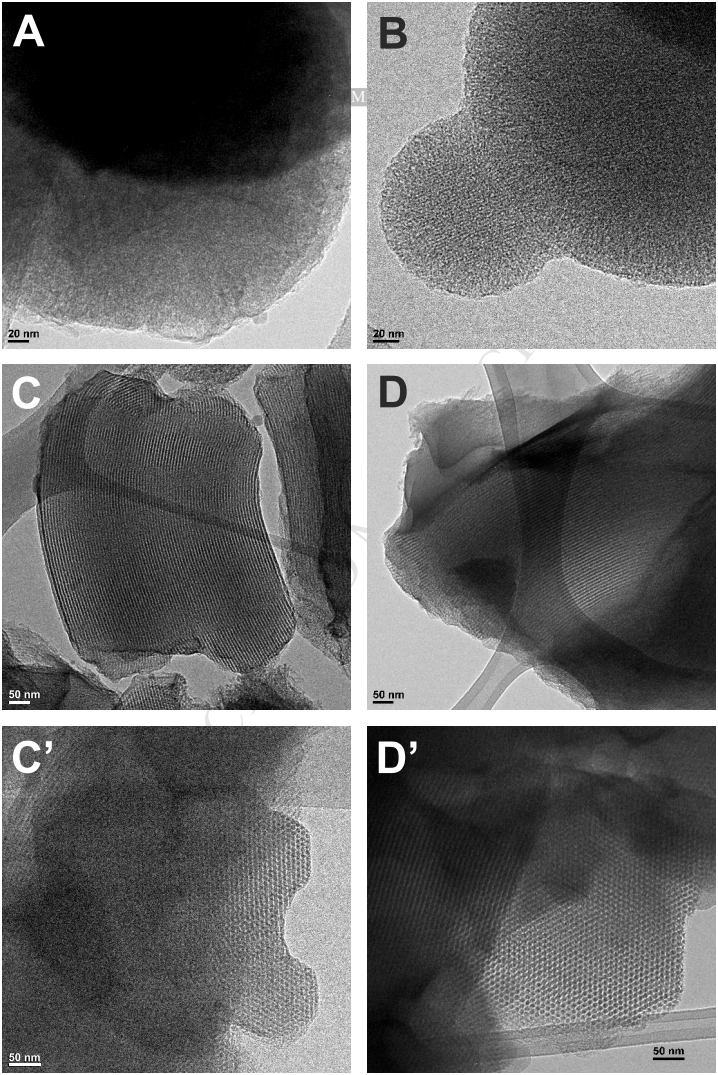
A
20 nm
B
20 nm
C
50 nm
D
50 nm
C'
50 nm
D'
50 nm

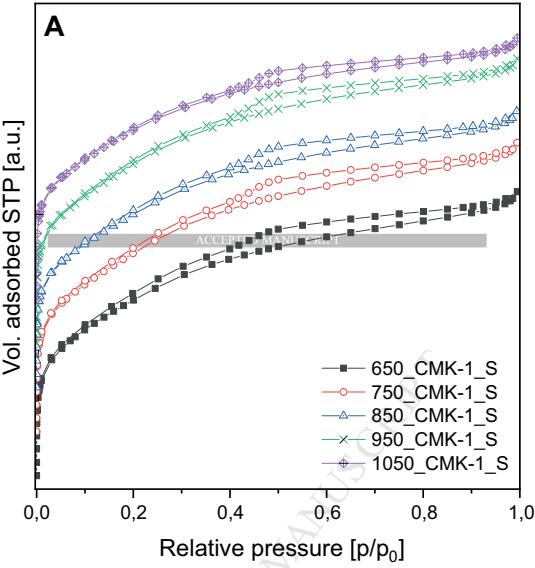
A
Vol. adsorbed STP [a.u.]
650_CMK-1_S
750_CMK-1_S
850_CMK-1_S
950_CMK-1_S
1050_CMK-1_S
0,0
0,2
0,4
0,6
0,8
1,0
Relative pressure [p/p0]

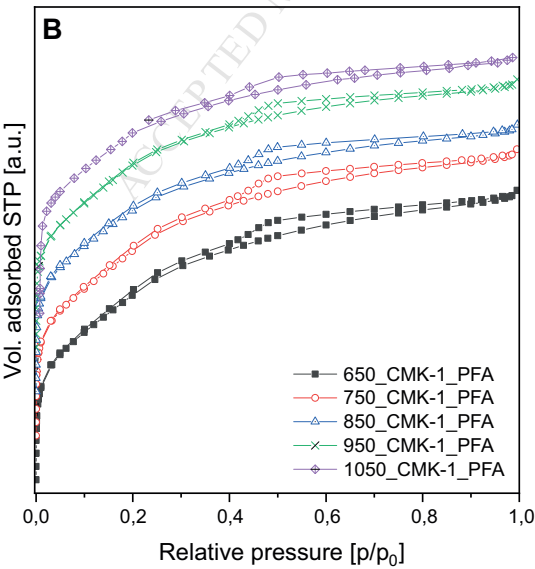
B
Vol. adsorbed STP [a.u.]
650_CMK-1_PFA
750_CMK-1_PFA
850_CMK-1_PFA
950_CMK-1_PFA
1050_CMK-1_PFA
0,0
0,2
0,4
0,6
0,8
1,0
Relative pressure [p/p0]

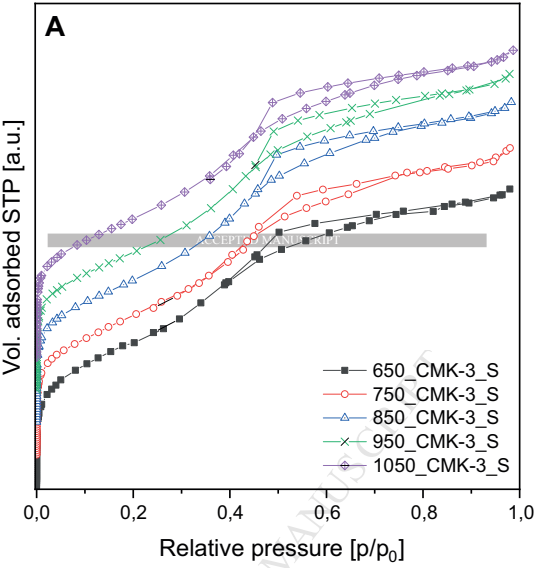
A
Vol. adsorbed STP [a.u.]
650_CMK-3_S
750_CMK-3_S
850_CMK-3_S
950_CMK-3_S
1050_CMK-3_S
0,0
0,2
0,4
0,6
0,8
1,0
Relative pressure [p/p0]

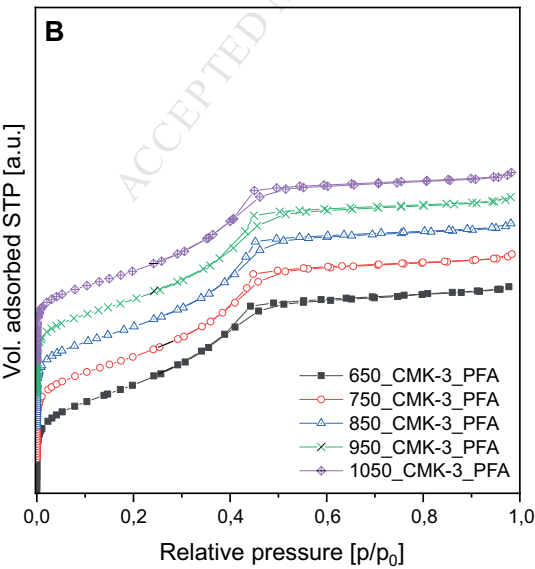
B
Vol. adsorbed STP [a.u.]
650_CMK-3_PFA
750_CMK-3_PFA
850_CMK-3_PFA
950_CMK-3_PFA
1050_CMK-3_PFA
0,0
0,2
0,4
0,6
0,8
1,0
Relative pressure [p/p0]

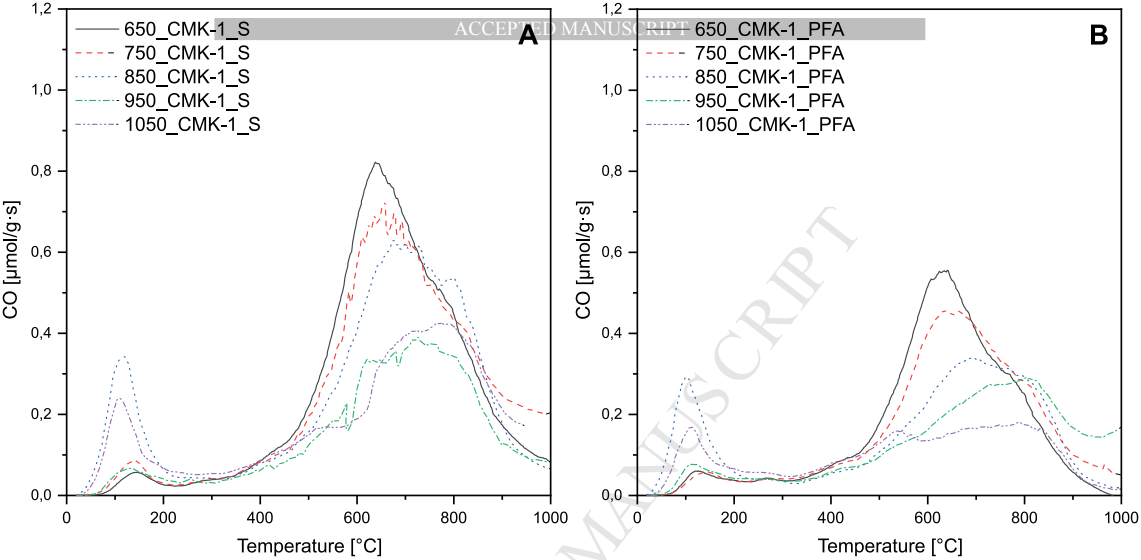

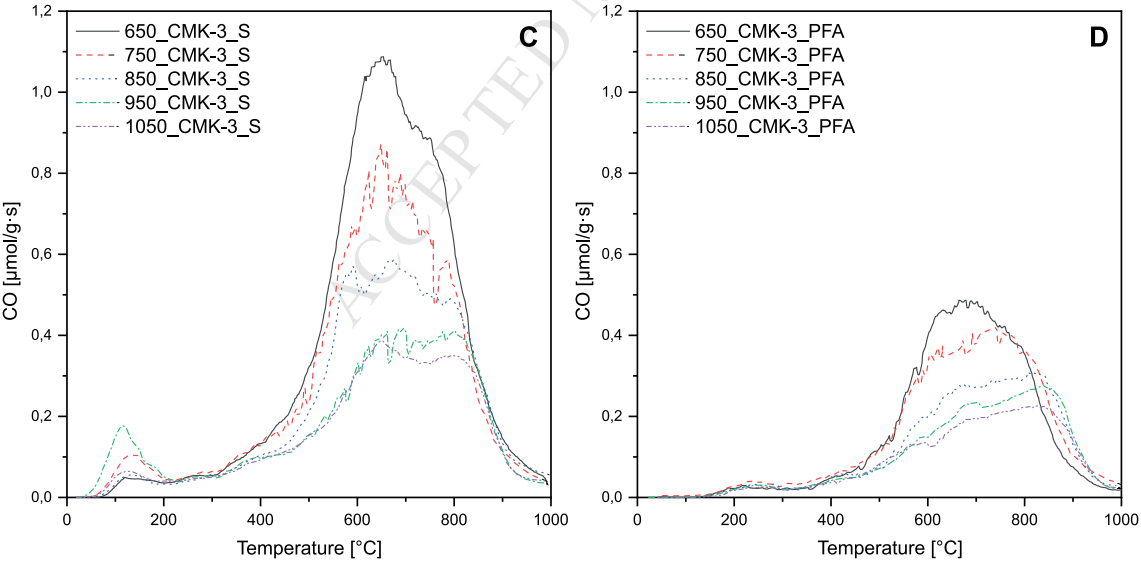

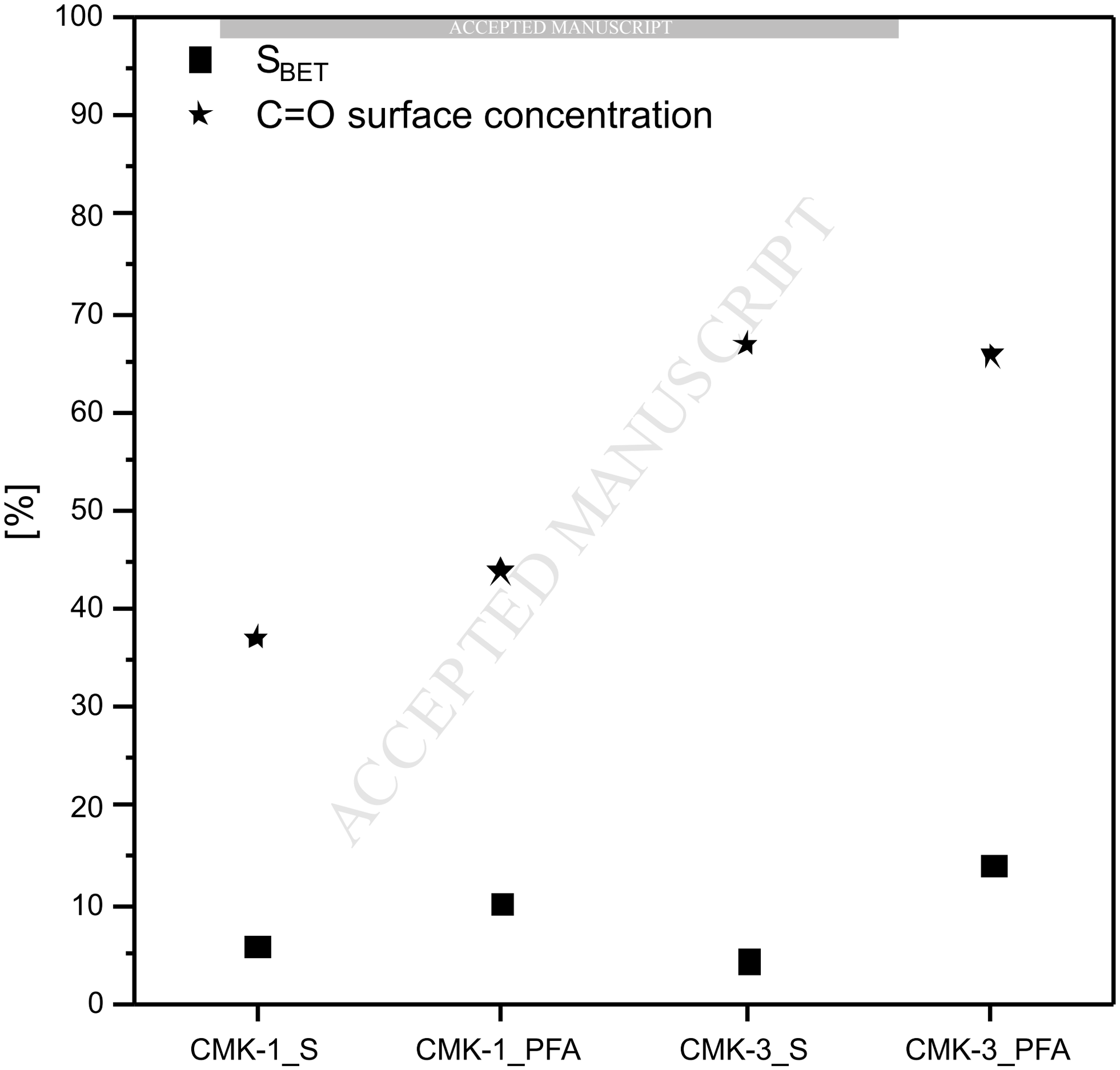

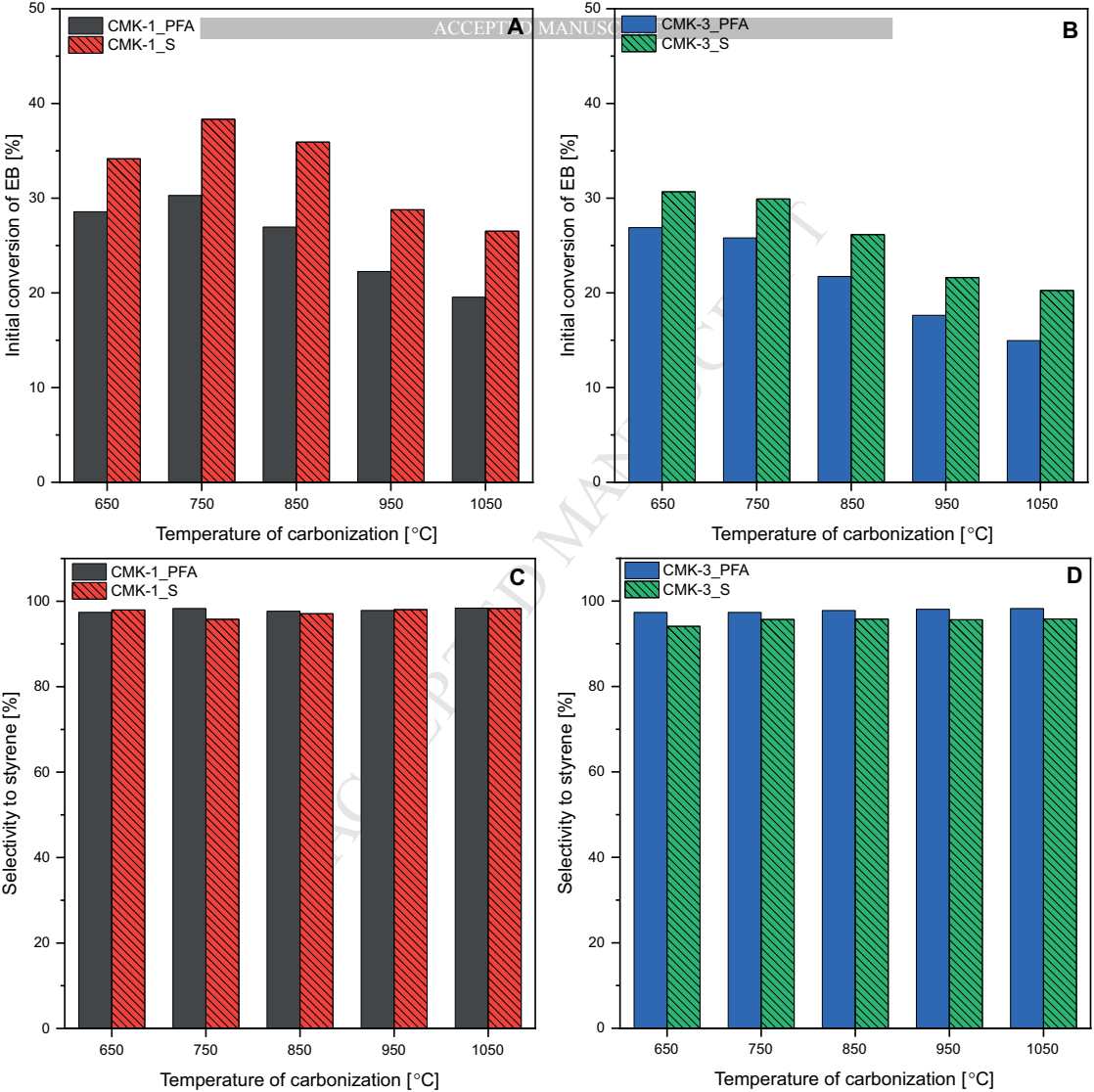

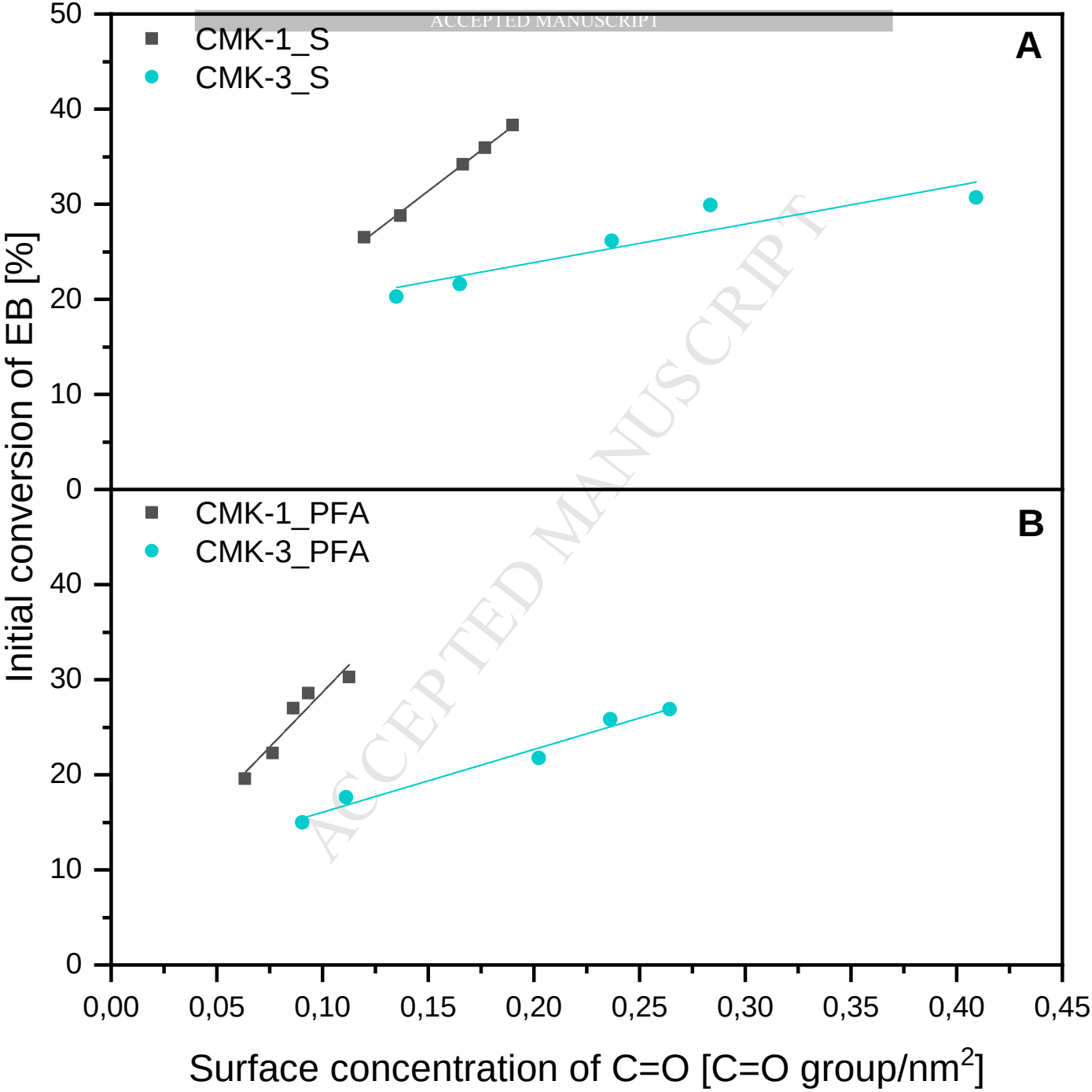

Highlights

- Pore filling influences shrinkage of carbon precursor/silica composite

- Sucrose-derived materials reveal larger shrinkage during carbonization

- CMK-1 is more active in oxidative dehydrogenation compared to CMK-3

- Regular pore arrangement in CMK-1 favors diffusion of reactant molecules

- Superficial C=O functionalities are utilized more efficiently for CMK-1